Zirconolite, chevkinite and other rare earth minerals from nepheline syenites and peralkaline granites and syenites of the Chilwa Alkaline Province, Malawi

R. G. PLATT

Dept. of Geology, Lakehead University, Thunder Bay, Ontario, Canada

F. WALL, C. T. WILLIAMS AND A. R. WOOLLEY

Dept. of Mineralogy, British Museum (Natural History), Cromwell Road, London SW7 5BD, U.K.

Abstract

Five rare earth-bearing minerals found in rocks of the Chilwa Alkaline Province, Malawi, are described. Zirconolite, occurring in nepheline syenite, is unusual in being optically zoned, and microprobe analyses indicate a correlation of this zoning with variations in Si, Ca, Sr, Th, U, Fe, Nb and probably water; it is argued that this zoning is a hydration effect. A second compositional zoning pattern, neither detectable optically nor affected by the hydration, is indicated by variations in Th, Ce and Y such that, although total *REE* abundances are similar throughout, there appears to have been *REE* fractionation during zirconolite growth from relatively heavy-*REE* and Th-enrichment in crystal cores to light-*REE* enrichment in crystal rims.

Chevkinite is an abundant mineral in the large granite–quartz syenite complexes of Zomba and Mulanje, and analyses are given of chevkinites from these localities. There is little variation in composition within each complex, and only slight differences between them; they are all typically light-*REE*-enriched. The Mulanje material was shown by X-ray diffraction to be chevkinite and not the dimorph perrierite, but chemical arguments are used in considering the Zomba material to be the same species. Other rare earth minerals identified are monazite, fluocerite and bastnäsite. These are briefly described and microprobe analyses presented.

KEYWORDS: zirconolite, chevkinite, monazite, fluocerite, bastnäsite, Chilwa Alkaline Province, Malawi.

Introduction

TEN relatively rare accessory minerals were identified during an investigation of the rock-forming, mafic minerals in peralkaline granites and syenites (Platt and Woolley, 1986) and nepheline syenites (Woolley and Platt, 1986) of the Chilwa Alkaline Province, Malawi. These minerals were zirconolite, chevkinite, monazite, rosenbuschite, catapleiite, lavenite, yttrian fluorite, britholite, fluocerite, and bastnäsite. The rare-earth-rich group, particularly zirconolite and chevkinite, proved to be especially interesting, the former because of the unusual element distribution in zoned crystals, as well as its relative rarity, the latter because of its abundance in several complexes. This paper describes these two minerals together with a number of other rare earth species.

The Chilwa Alkaline Province is located in Southern Malawi and adjacent part of Mozambique, at the southern end of the East African Rift system. It comprises intrusions of peralkaline granite and syenite, nepheline syenite and carbonatite. A general map of the province can be found in Woolley and Garson (1970, Fig. 2), and a larger scale map of the area from which the minerals described in this paper were collected is given by Woolley and Platt (1986, Fig. 1).

Analytical techniques

The mineral compositions were determined by electron microprobe analysis using a Cambridge Instruments Microscan 9 wavelength-dispersive microanalyser operated at 20 kV with a specimen current of 25 nA and using minerals, oxides, or pure

Mineralogical Magazine, June 1987, Vol. 51, pp. 253–263

metals as standards. Corrections were made for overlaps between rare earth elements (*REE*) and between Dy-$L\alpha_1$ and Mn-$K\beta_1$, and Ba-$L\alpha_1$ and Ti-$K\alpha_2$ by using empirical overlap factors calculated in a similar manner to that of Åmli and Griffin (1975). For further discussion on microprobe analysis of *REE* see Roeder (1985). It should be noted that in light-*REE* (*LREE*)-enriched minerals, the overlap corrections applied to Pr-$L\alpha_1$, Sm-$L\alpha_1$, Eu-$L\alpha_1$ and Gd-$L\alpha_1$ (for the elements Ce and La) are large relative to the weight percent (wt.%) concentrations of these elements.

The microprobe analysis quoted for monazite is a hybrid of wavelength- and energy-dispersive analyses. This was found to be necessary as the wavelength-dispersive instrument gave high totals, apparently due to the Microscan 9 ZAF program calculating *LREE* (particularly La) concentrations which are too high in the presence of large phosphorous values. The La figure quoted for monazite in Table 3 is the average of analyses from two separate energy-dispersive microprobes.

To characterize the zoning in zirconolite, incremental spot analyses (step scans) were carried out across the grains to obtain count rates for seven selected elements at each point in the traverse. Using background and ZAF factors obtained from the full analyses, the raw data were corrected to give wt.% oxides of the appropriate elements.

Semi-quantitative F and C analyses were performed on the Jeol 733 Superprobe in the Department of Materials Science, University of Bath. The instrument was operated at 10 kV with a beam current of 1.7 nA using SrF_2 and graphite as standards.

Zirconolite

Zirconolite has been identified in a specimen of nepheline syenite from Chikala, the most easterly of a line of four overlapping nepheline syenite–syenite complexes in the northern part of the Chilwa Alkaline Province (Woolley and Platt, 1986). The rock was collected by M. S. Garson from close to the outer contact on the southeastern side of the complex, northwest of Mposa Village. The analysed specimen, now in the British Museum (Natural History) and numbered BM 1980, P23(1), was cut from the Garson specimen in the Malawi Geological Survey Collection (No. G964).

Petrography. The normal nepheline syenites of Chikala, and the similar complexes further west, are coarse rocks with abundant amphibole and pyroxene, but the zirconolite-bearing rock is unusual in containing neither amphibole nor pyroxene, and by being fine grained. It is a nepheline syenite containing subhedral alkali feldspar, ragged patches of turbid nepheline, which is sometimes included in the feldspar and partly altered to sericite, and abundant brown biotite; an opaque oxide phase is plentiful, as is apatite. Zirconolites vary in size from less than 30 μm up to 300 μm in diameter. Smaller grains are anhedral with a dark red-brown colour, whereas larger grains are subhedral to euhedral and invariably zoned optically with pale brown, nearly transparent cores and dark brown, nearly opaque rims (Fig. 1*a*). The colour transition is usually sharp. In some crystals the colour is patchy, light to

TABLE 1. Microprobe analyses of zirconolites

	Light Core (average of 3)	Dark Core (1 only)	Rim (average of 3)	Unzoned anhedral grains (average of 2)	(1 only)
	"LC"	"DC"	"AR"	"A,D"	"C"
MgO	0.05	0.18	0.13	0.09	0.11
Al_2O_3	0.43	0.75	0.89	0.68	0.56
SiO_2	3.25	<.07	<.07	<.07	<.07
CaO	1.83	7.22	8.08	8.43	10.03
TiO_2	24.8	26.0	27.2	27.8	28.3
MnO	0.54	0.50	0.28	0.28	0.21
FeO+	4.56	8.32	7.96	8.47	7.66
SrO	0.19	<.05	<.05	0.06	<.05
Y_2O_3	3.70	3.83	3.23	3.33	1.84
ZrO_2	27.3	27.3	28.8	29.2	29.4
Nb_2O_5	6.9	8.1	8.3	8.2	9.6
BaO	<.06	0.06	<.06	0.10	<.06
La_2O_3	0.34	0.40	0.53	0.54	0.64
Ce_2O_3	1.57	1.85	2.54	2.97	3.23
Pr_2O_3	0.41	0.43	0.49	0.56	0.47
Nd_2O_3	3.61	3.97	3.98	4.49	3.96
Sm_2O_3	0.98	0.79	0.76	0.78	0.61
Eu_2O_3	0.26	0.30	0.33	0.35	0.31
Gd_2O_3	1.09	0.86	0.86	0.84	0.44
Dy_2O_3	1.12	0.99	0.75	0.75	0.36
Er_2O_3	0.52	0.41	0.35	0.40	0.13
Yb_2O_3	0.60	0.49	0.39	0.31	0.22
HfO_3	0.40	0.43	0.44	0.59	0.81
Ta_2O_5	0.77	0.69	0.59	0.33	0.70
ThO_2	7.37	4.32	1.62	0.89	0.38
UO_2	1.82	0.98	0.57	0.28	0.13
TOTAL	94.41*	99.17	99.07	100.72	100.10
$\Sigma\left(\frac{REE_2O_3+}{Y_2O_3}\right)$	14.60	14.32	14.21	15.32	12.21
	Number of cations based on 7 oxygens				
Ca	.117	.524	.573	.589	.691
Y	.117	.138	.114	.116	.063
Sr	.007	-	-	.002	-
Ba	-	.002	-	.003	-
La	.007	.010	.013	.013	.015
Ce	.034	.046	.062	.071	.076
Pr	.009	.011	.012	.013	.011
Nd	.077	.096	.094	.105	.091
Sm	.020	.018	.017	.018	.014
Eu	.005	.007	.007	.008	.007
Gd	.022	.019	.019	.018	.009
Dy	.022	.022	.016	.016	.007
Er	.010	.009	.007	.008	.003
Yb	.011	.010	.008	.006	.005
Th	.100	.067	.024	.013	.006
U	.024	.015	.014	.004	.002
Σ Ca	.582*	.994	.980	1.003	1.000
Zr	.793	.902	.928	.927	.921
Hf	.007	.008	.008	.011	.015
Σ Zr	.800	.910	.936	.938	.936
Mg	.004	.018	.013	.009	.011
Al	.030	.060	.069	.052	.042
Si	.194	-	-	-	-
Ti	1.113	1.325	1.353	1.365	1.370
Mn	.027	.029	.016	.015	.011
Fe	.227	.472	.440	.462	.412
Nb	.187	.248	.247	.241	.280
Ta	.012	.013	.011	.006	.015
Σ Ti	1.794*	2.165	2.149	2.150	2.141
TOTAL	3.169*	4.069	4.065	4.089	4.077

*Low totals due to probable high H_2O content (see text)
+All Fe as FeO

dark in the core, although the rims are always dark.

Nomenclature and structure. Zirconolite is isochemical with the minerals zirkelite and polymignite, though structurally distinct (Mazzi and Munno, 1983; White, 1984). Structural characterization is difficult because of the small grain size and/or metamict nature of these minerals, and also because they may be intergrown (Mazzi and Munno, 1983).

Powder diffraction photographs were taken of material from two of the larger grains removed from thin sections. One predominantly dark grain, gave a weak powder pattern corresponding to partially metamict zirconolite or zirkelite, which can only be distinguished from each other by single-crystal study of non-metamict material (Mazzi and Munno, 1983). The other grain, predominantly pale, did not give a discernible X-ray pattern. After heating to 800 °C however, a weak pattern was obtained identical to that of the dark grain. The pale mineral is therefore a metamict variant of zirconolite or zirkelite. In accordance with recent practice when structural characterization of these minerals has not been possible, the name zirconolite is preferred to that of zirkelite, and is used in this report.

The generalized formula of zirconolite can be expressed as $AB_xC_{3-x}O_7$, where A = Ca, Y, Sr, Ba, *REE*, Th and U in 8-coordination, B = Zr and Hf in 7-coordination, and C = Ti, Mg, Al, Si, Mn, Fe, Nb, and Ta in three distinct sites, two 6- and one 5-coordination (Gatehouse *et al.*, 1981; Kesson *et al.*, 1983). The cation distribution given here (Table 1) is different from that outlined by Frondel (1975), and subsequently used by Williams (1978), since Fe^{2+} is here assigned to one of the three Ti sites with Y, *REE*, Th and U occupying the Ca site. This corresponds to chemical and structural refinement data of Gatehouse *et al.* (1981) and Kesson *et al.* (1983) on synthetic zirconolites.

Zoning. Over 50 electron microprobe analyses of zirconolites, including a number of traverses across zoned crystals, were carried out, and several X-ray distribution maps recorded. A selection of analyses is given in Table 1. Two distinct compositional zoning patterns are present in zirconolite (Figs. 1*a–f* and 2):

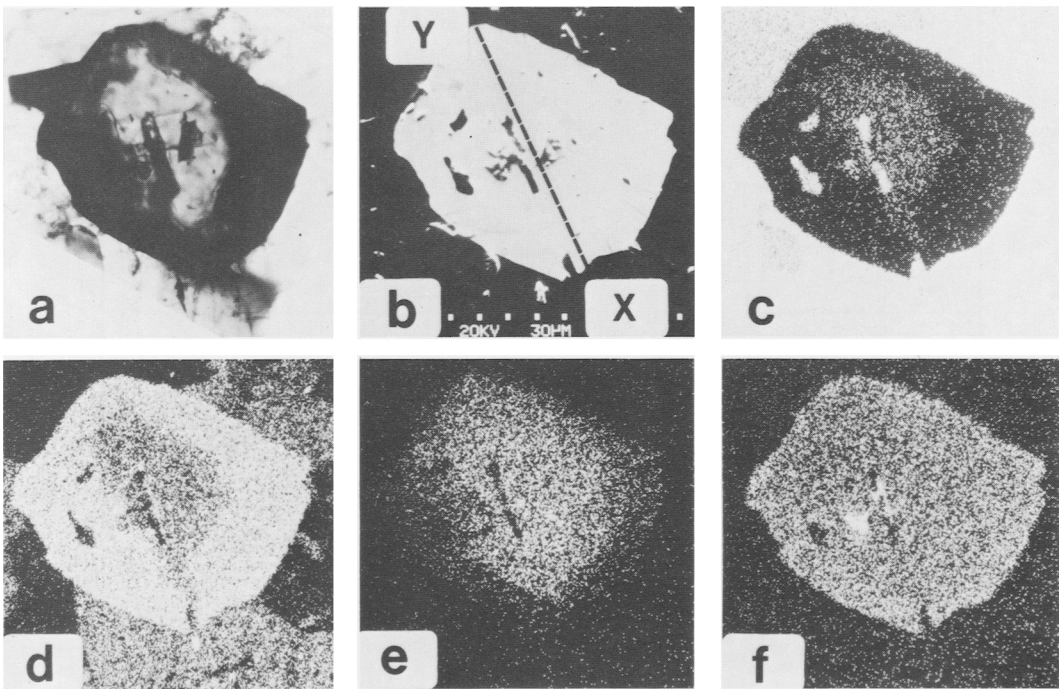

FIG. 1. (*a*) photomicrograph, (*b*) secondary electron image, (*c*)-(*f*) X-ray distribution images of euhedral zirconolite showing both optical and chemical zoning, (*c*) = Si, (*d*) = Ca, (*e*) = Th, (*f*) = Ce. Points X and Y mark the extremities of the step scan traverse plotted in Figs. 2, 3, and 4. The silicate inclusions in the zirconolite grain are biotite; the Ce-rich inclusion is an unidentified non-silicate phase. Associated with the zirconolite are biotite, alkali feldspars and nepheline.

1. Optical zoning. There is a clear correlation between the optical zoning and the concentrations of several elements including Si and Ca (Figs. 1*c* and *d* and 2). Where the colour variation is patchy in the core region, a comparison of microprobe analyses of the light and dark areas (Table 1) shows that SrO, ThO_2 and UO_2 are enriched, whilst FeO and Nb_2O_5 are depleted in the light areas, but there is little or no variation in the *REE*. In addition, full microprobe analyses of the light regions for elements of atomic number 11 and above have low totals, ranging from 93 to 96 % (Table 1), suggesting the presence of several wt. % of low atomic number elements. F and C were sought using the Jeol 733 Superprobe (H could not be detected), but were below the detection limit of the instrument i.e. less than approximately 0.5 wt. %. Hydrogen, as H_2O, is the most probable unanalysed element present in the pale core region at concentration levels of several wt. %.

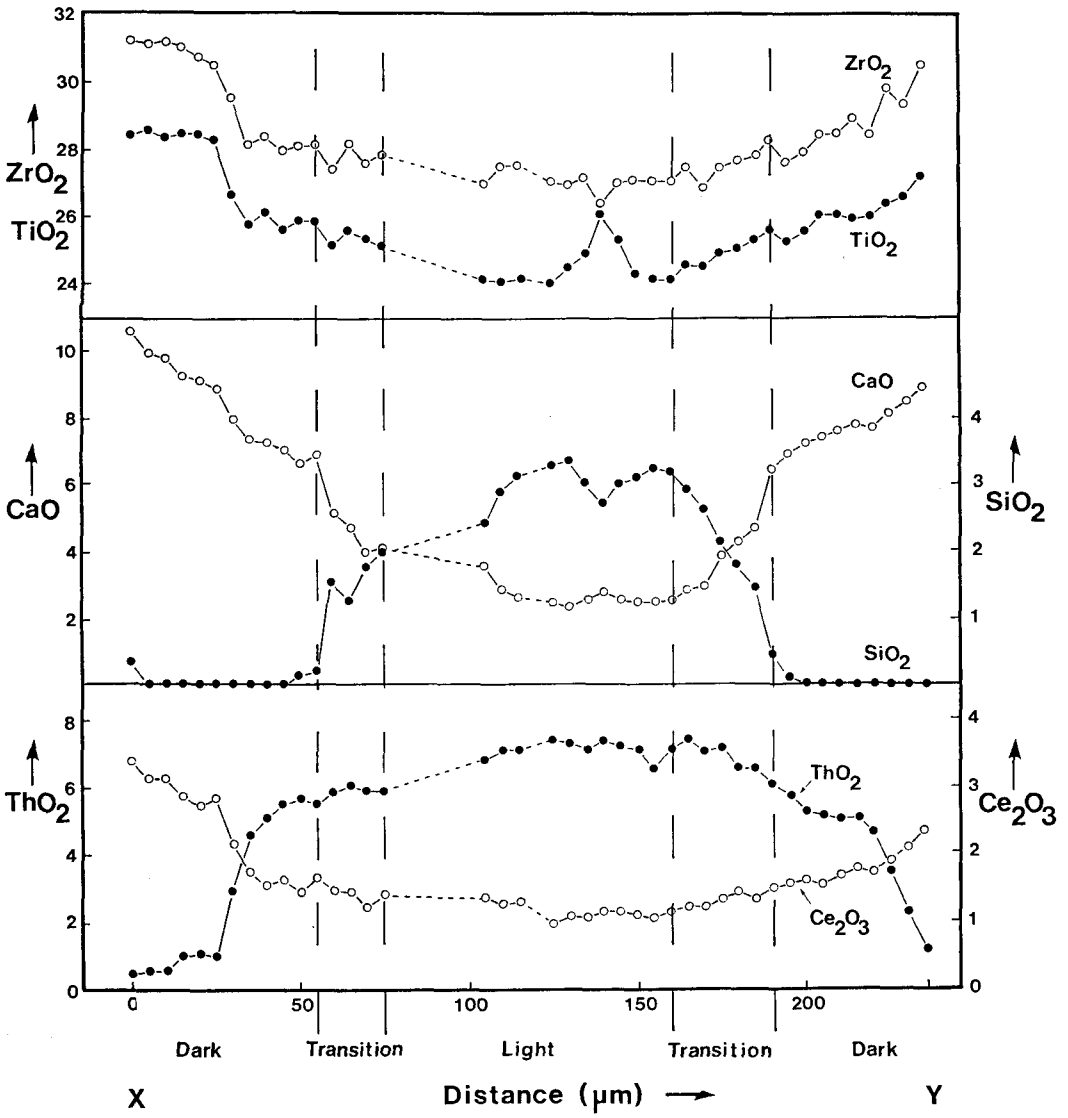

FIG. 2. Concentrations of various elements (wt. % oxides) in zirconolite plotted against distance along the X–Y traverse shown in Fig. 1. The 'dark', 'transition' and 'light' zones refer to the optical characteristics of the crystal.

Borodin *et al.* (1960) analysed for SiO_2 and H_2O in zirconolites from the Arbarastkh alkaline complex, Alden, USSR, and noted a similar chemical correlation with colour. Light brown zirconolites contain significantly higher SiO_2 and H_2O than the coexisting dark brown variety. Borodin *et al.* (1960) also observed differences in S.G. and R.I. between the light and dark varieties. A combination of these physical and chemical differences suggests that the pale variety is a hydrated metamict variant of the dark brown zirconolite. The highest concentrations of U and Th are confined to the pale brown regions of the Chikala zirconolite and would cause α-radiation damage to the structure and produce metamict zirconolite (e.g. Mitchell, 1973), although a high degree of short-range order would still be retained (Sinclair and Ringwood, 1981). Varying amounts of water could then be accommodated in the partially ordered structure with the loss of other elements. These effects have been observed in experimental studies on natural zirconolites. Kesson and Ringwood (1983) have shown that in the presence of deionised water, Ca is leached from the zirconolite structure, presumably with the addition of water, although other elements such as U, remain relatively immobile.

2. REE zoning. The second compositional zoning pattern can be seen in the variations of ThO_2 and Ce_2O_3 and Y_2O_3 (Figs. 1*e*,*f* and 2). By comparing the average rim analysis with the dark core analysis in Table 1 (the dark core analysis is preferred to the light core analysis in this comparison as it is apparently unaffected by hydration), it can be seen that Y_2O_3 and ThO_2 are enriched, and CaO and Ce_2O_3 depleted in the core relative to the rim. The other elements do not show significant variations, suggesting that a relatively simple substitution is occurring in the Ca site only, and that it is not necessary to invoke the entry of smaller *HREE* ions into the Zr site, as has been described for other zirconolites (Ringwood, 1985).

The variations in Th, Ce, and Y are seen in the ternary diagram (Fig. 3) to be inter-related. Data from the step scan along X–Y in Fig. 1 are plotted in both Figs. 3 and 4, together with a shaded area enclosing data points from another four zoned crystals. Average compositions of rims, cores and unzoned anhedral grains (Table 1) are also plotted in Figs. 3 and 4. The ternary diagram (Fig. 3) shows a well-defined core region with the compositional zoning displaying an arcuate trend. Several smaller unzoned, anhedral grains have compositions which plot within the rim compositions (Fig. 3); these probably represent the outer sections of larger zoned crystals.

A plot of $(Ce/Y)_{cn}$ (cn = chondrite-normalized)

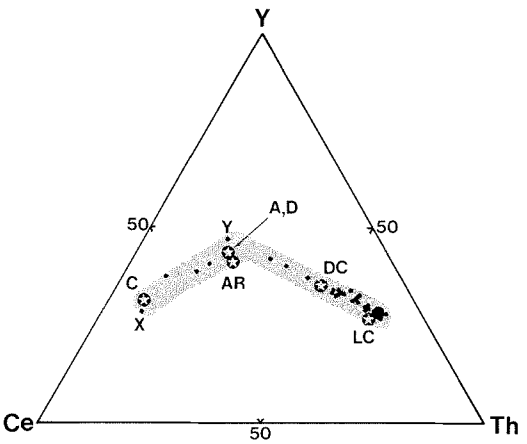

FIG. 3. Ce–Y–Th ternary diagram (wt.%) for zirconolites. The dots represent data from the traverse in Fig. 1 points X and Y mark the extremities of the traverse. The shaded area corresponds to > 90% of data points from traverses of four other zoned crystals. The starred symbols relate to the analyses in Table 1.

against ThO_2 (Fig. 4) illustrates fractionation in the *REE* during zirconolite growth, from relatively heavy-*REE* (*HREE*)-enrichment in the core, $(Ce/Y)_{cn} \leqslant 1$, to *LREE*-enrichment at the rims, $(Ce/Y)_{cn} > 1$. The rate of fractionation, however, was not constant during the growth of the zirconolite as there is only a very small increase in $(Ce/Y)_{cn}$ for a large increase in SiO_2 in the core (Fig. 4). The greatest variation in $(Ce/Y)_{cn}$ corresponds to the crystal rim, and in all cases the largest $(Ce/Y)_{cn}$ value occurs at the outermost analysed crystal edges.

The total *REE* abundances are similar for both core and rim samples (Table 1), but when plotted on a

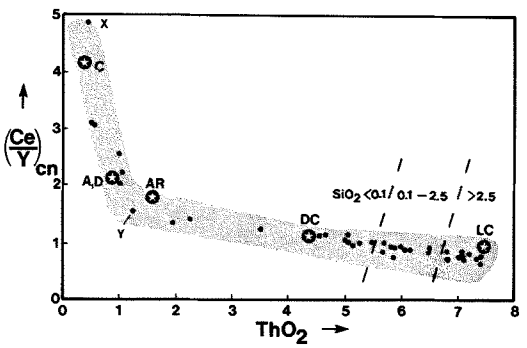

FIG. 4. $(Ce/Y)_{cn}$ against ThO_2 (wt.%) for zirconolites. The symbols are the same as in Fig. 3. For a discussion on SiO_2 variation, see text.

chondrite-normalized diagram (Fig. 5*a*), the fractionation effect becomes apparent. Although the patterns are similar and comparable in shape to *REE* chondrite-normalized plots of zirconolites from some other localities (Fowler and Williams, 1986), the core is both *LREE*-depleted and *HREE*-enriched relative to the rim, and pivots about the position of Nd.

Discussion. Purtscheller and Tessadri (1985) discuss two possible mechanisms of zirconolite formation and zoning: (1) crystallization directly from a differentiated magma, and (2) crystallization

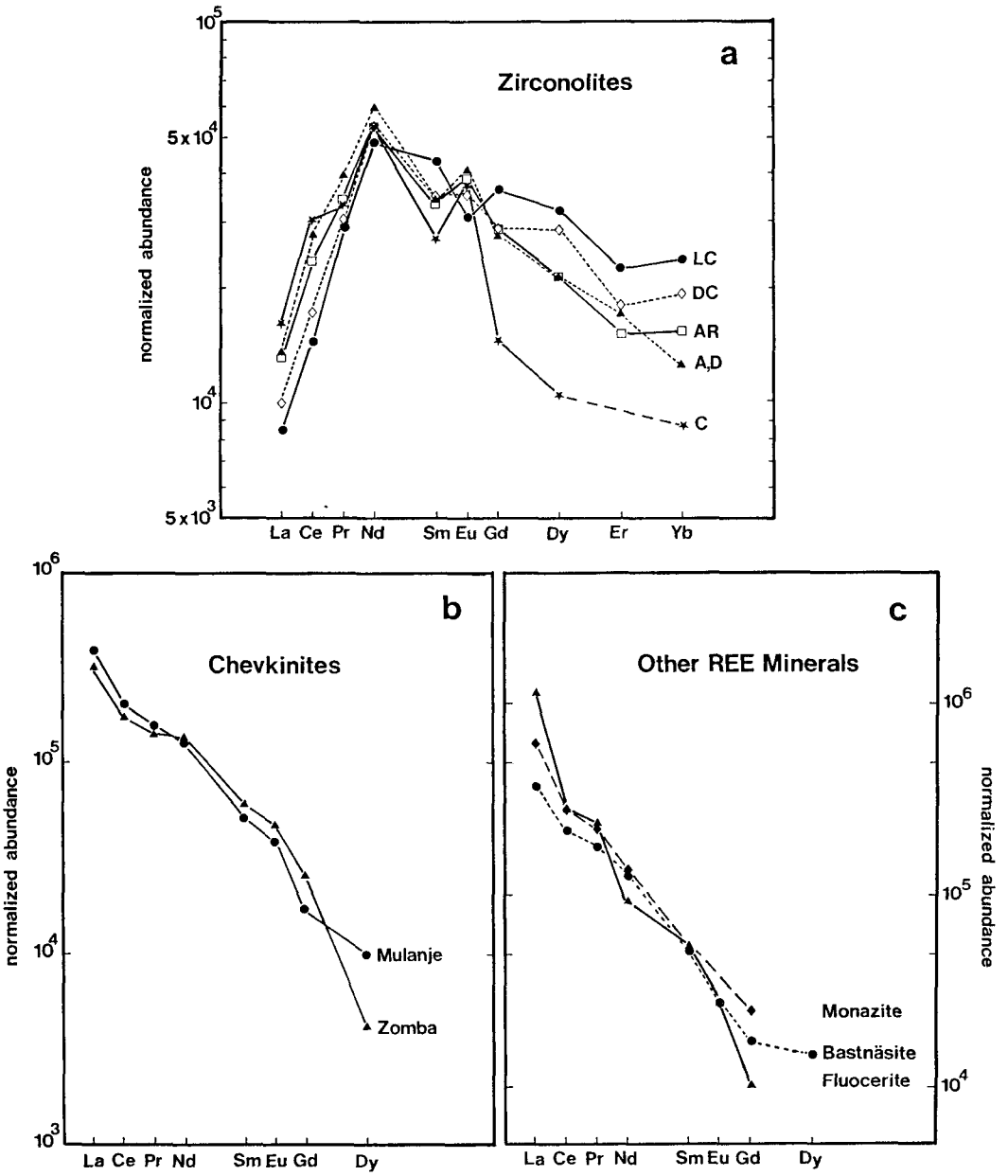

FIG. 5. Chondrite-normalized *REE* plots for the samples given in Tables 1, 2 and 3; (*a*) zirconolites, (*b*) chevkinites and (*c*) other *REE* minerals. Chondrite values after Wakita *et al.* (1971).

by metamorphic reaction (Raber and Haggerty, 1979) involving carbonates and Ti and Zr minerals. The zirconolites from Malawi are undoubtedly of magmatic origin and are not a consequence of metamorphic reactions.

It is proposed that the two types of zoning described here resulted from separate events. Initial crystallization of zirconolite incorporated high concentrations of Th and U into the mineral which produced a metamict variety. Fractionation of the *REE* accompanied the crystallization of the rims, perhaps in a locally restricted environment (Williams, 1978), and resulted in an outward increase of *LREE*-enrichment, accompanied by lower Th and U contents in the rim region. At some stage there was a gain in SiO_2 and H_2O in the core, and a subsequent loss of other elements, including CaO and FeO, from the metamict core producing the pale brown zones. It is not known whether this stage occurred before crystallization of the rims during an intermediate hydration stage, or as a late-stage event, during which these elements moved by way of microcracks in the crystalline rim.

Using the zirconolite thermometer of Wark *et al.* (1973) and Raber and Haggerty (1979) based on the Ti/Zr cation ratio, the zoned zirconolite grain shows little variation in crystallization temperature from core to rim. Actual temperatures have not been calculated as previous workers have shown that temperatures computed from the zirconolite

TABLE 2. Microprobe analyses of chevkinites

	Mulanje, in quartz syenite BM1984,P29(9)		Zomba, in quartz syenite BM1980,P18(13)	
	Average of 4 analyses	Range	Average of 6 analyses	Range
MgO	<0.05	<0.05	<0.05	<0.05
Al_2O_3	<0.05	<0.05	0.16	0.11 - 0.18
SiO_2	19.0	19.0 - 20.0	19.5	18.8 - 20.0
CaO	1.20	1.05 - 1.38	3.31	3.14 - 3.49
TiO_2	16.8	16.1 - 17.4	17.5	17.3 - 17.7
MnO	<0.08	<0.08	<0.08	<0.08
FeO^+	11.2	10.5 - 11.6	11.2	11.1 - 11.4
SrO	0.05	<0.05 - 0.08	<0.05	<0.05
Y_2O_3	0.10	0.08 - 0.10	0.57	0.53 - 0.62
ZrO_2	0.14	<0.05 - 0.20	0.82	0.57 - 0.91
Nb_2O_5	0.71	0.64 - 0.79	1.6	1.6 - 1.7
BaO	0.41	0.09 - 0.20	0.16	0.11 - 0.20
La_2O_3	15.9	15.4 - 16.9	13.0	12.5 - 13.7
Ce_2O_3	22.1	21.6 - 22.0	18.6	18.1 - 18.9
Pr_2O_3	2.2	2.1 - 2.3	2.0	1.9 - 2.2
Nd_2O_3	9.8	8.8 - 10.2	10.1	9.7 - 10.6
Sm_2O_3	0.96	0.78 - 1.07	1.38	1.12 - 1.61
Eu_2O_3	0.32	0.28 - 0.4	0.4	0.3 - 0.5
Gd_2O_3	0.52	0.39 - 0.60	0.77	0.51 - 1.0
Dy_2O_3	0.34	0.21 - 0.34	0.15	0.15 - 0.23
Yb_2O_3	<0.15	<0.15	<0.15	0.15
ThO_2	0.08	<0.07 - 0.23	0.60	0.47 - 0.74
UO_2	<0.06	<0.06	0.07	<0.06 - 0.12
TOTAL	101.56		101.89	
Σ ($REE_2O_3+Y_2O_3$)	52.24		49.97	
	Number of cations based on 22 oxygens			
La	1.247		0.988	
Ce	1.720		1.403	
Pr	0.171		0.151	
Nd	0.744		0.743	
Sm	0.070		0.067	
Eu	0.023		0.028	
Gd	0.037		0.053	
Dy	0.023		0.010	
Y	0.011		0.062	
Th	0.004		0.028	
U	0.002		0.003	
Ba	0.012		0.013	
^{IX}Ca	"		0.451	
	4.064		4.000	
^{VI}Ca	0.273		0.279	
Fe	1.992		1.929	
Ti	2.686		2.711	
Zr	0.018		0.082	
Nb	0.068		0.149	
Al			0.039	
Mn				
	5.037		5.189	
Si	4.040		4.016	

+All Fe as Fe^{2+}

thermometer are consistently higher than those indicated by field or petrological evidence (Purtscheller, and Tessadri, 1985; Raber and Haggerty, 1979). For a discussion of *P–T* conditions in the Chilwa Alkaline Province see Platt and Woolley (1986) and Woolley and Platt (1986).

Chevkinite

The *REE*-Fe-Ti silicate, chevkinite is a characteristic accessory mineral of some peralkaline granites, syenites, volcanic, and metasomatic rocks. For a list of reported chevkinite occurrences see Gmelin Handbook (1984) and Vlasov (1966). Some chevkinite compositions have a dimorph, perrierite, so that it can be difficult to identify chevkinite using chemical data alone.

Occurrence and petrography. Chevkinite has been found to be a relatively common phase in the more peralkaline granites and quartz syenites of the large syenite–granite complexes of Zomba and Mulanje. The mafic minerals of Mulanje have been described in some detail by Platt and Woolley (1986) and the mineralogy of Zomba is presently being investigated by Jones and Woolley. Chevkinite has also been identified in a quartz syenite from Chikala. Chevkinites from two rocks have been analysed. The first (BM 1980, P18(13)), from close to the road which climbs Zomba Mountain at its southern end, is a quartz syenite (15% normative quartz) of subhedral perthite prisms, aegirine-augite, an arfvedsonitic amphibole, altered fayalite, an opaque oxide phase and abundant zircon. There are patches and stellate clusters of late, fibrous alkali amphibole. Chevkinite forms occasional opaque to very dark reddish-brown stubby, euhedral to subhedral prisms.

The second chevkinite-bearing rock (BM 1984, P29(9)) is from a boulder collected in the Ruo river, about 200 m upstream from the hydro-electric plant, at the southern end of Mulanje. The rock is a quartz syenite of anhedral perthite, abundant quartz, arfvedsonitic amphibole, and an opaque oxide phase. Chevkinite is plentiful as stubby, euhedral, opaque prisms, and as irregularly shaped crystals which are commonly included in amphibole and are pleochroic from opaque to deep reddish brown.

Composition. The compositions of the chevkinites vary little within each rock; they are unzoned and there are only slight differences between the Zomba and Mulanje samples (Table 2), the Zomba chevkinite having slightly higher Ca, Ti and Th, and lower *REE*. The chondrite-normalized plots for the Zomba and Mulanje chevkinites show a smooth *LREE*-enriched pattern (Fig. 5*b*). All chevkinites are typically *LREE*-enriched although the amounts of the most abundant *LREE* vary (Gmelin Handbook, A8, 1984) and some chevkinites have Eu anomalies (for example, Reed 1986).

Chevkinite vs. perrierite. A grain of analysed Mulanje material was removed from a thin section and confirmed as chevkinite by X-ray powder diffraction. The Zomba grains, however, are too small for this procedure and the following discussion attempts to classify them on the grounds that chevkinite and perrierite are dimorphous only within certain compositional ranges. These ranges depend on the size of the cations occupying the *A* and the *B* and *C* sites where *A* = *REE*, Th, Ca, Sr, Na, and K, *B* = Fe^{2+}, Mg, Mn, and Ca, and *C* = Ti, Fe^{3+}, Fe^{2+}, Mg, Mn, and Al in the formula $A_4(B,C)_5Si_4O_{22}$ (Ito and Arem, 1971; Ito, 1967;

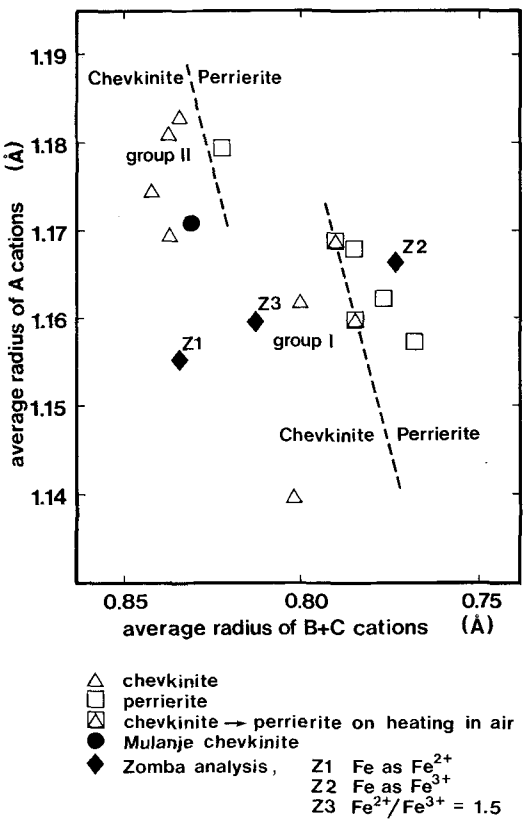

FIG. 6. Distribution of natural perrierites and chevkinites as a function of average ionic radius of the *A* and *B*+*C* sites after Segalstad and Larsen (1978) using the data of Shannon and Prewitt (1969) for cationic radii in 6-fold coordination for all cations. Group I has low Al and little or no Ca in *A* sites. Group II has all or most Ca accommodated in *A* sites.

Calvo and Faggiani, 1974). Fig. 6 is a plot of the average ionic radius of *A* cations against the average ionic radius of *B* and *C* cations for the Mulanje and Zomba analyses and for 12 natural chevkinites and perrierites given in Segalstad and Larsen (1978). They found that the 12 analyses formed 2 groups with different chevkinite-perrierite boundaries. Group I on Fig. 6 has all Ca accommodated in *A* sites whereas group II has most Ca located in *B* and *C* sites. The Mulanje chevkinites (confirmed as chevkinite) has all its Ca in *B* and *C* sites and plots with group II, Fig. 6. The Zomba analysis (unconfirmed) is different, however, because its lower *REE* content and higher Ca result in 60% of the Ca cations being assigned to *A* sites. Therefore it resembles group I and plots well within the chevkinite field for this group (Z1 on Fig. 6). However, all the Fe in the Zomba analysis has been assumed to be Fe^{2+}, which may not be correct. Positions Z2 and Z3 on fig. 6 show the effect of converting Fe^{2+} to Fe^{3+}: Z2 has all Fe as Fe^{3+} (unlikely to be correct as this gives a total of 103.1 wt.%) and Z3 has the Fe distributed to give a cation total of 13.0 (total 102.4 wt.% and so likely to be an upper estimate of Fe^{3+} content). Because Z1 and Z3 are both well within the chevkinite field it is concluded that the Zomba mineral is most likely to be chevkinite.

Other rare earth minerals

Three other rare earth minerals, monazite, fluocerite and bastnäsite were identified in a peralkaline granite (sample BM 1984, P29(74)) from Mulanje. The rock is composed primarily of perthite, quartz, arfvedsonite and aenigmatite, with minor aegirine. The rare earth minerals occur intergrown one with another as aggregates approximately 0.6 mm in size. Phases from two such aggregates were analysed; one within an aenigmatite grain, and one associated with quartz.

Monazite. Monazite occurs mostly intergrown with fluocerite and bastnäsite, but two separate grains were identified at the edge of the aenigmatite grain. The larger was subhedral, 130 by 60 μm, and pale yellow. Five spot analyses of this grain show little variation and the average analysis is given in Table 3. The chondrite-normalized (Fig. 5*c*) *REE* pattern is strongly *LREE*-enriched and is comparable to monazites from similar geological environments (Fleischer and Altschuler, 1969).

Fluocerite. Another transparent, yellow rare earth mineral (150 μm in diameter) was identified as fluocerite (Ce,La)F_3 by X-ray powder diffraction of material removed from thin section. A microprobe analysis of this mineral, an average of three spot analyses, is given in Table 3, and the chondrite-

Table 3. Microprobe analyses of other rare earth minerals

All from peralkaline granite BM1980,P29(9)

	Monazite (average of 5)	***		Fluocerite (average of 3)	Bastnäsite (+ Ti-Fe oxide mixture) (average of 4)
MgO	<0.05	-		<0.05	<0.05
Al_2O_3	<0.05	-		<0.05	<0.05
SiO_2	1.24	.0489	.9944	0.29	0.61
P_2O_5	28.3	.9495		<0.05	0.06
CaO	<0.05	-		0.21	0.39
TiO_2	<0.05	-		<0.05	19.5
MnO	<0.05	-		<0.05	<0.05
FeO+	<0.05	-		<0.05	9.84
SrO	<0.05	-		<0.05	0.08
Y_2O_3	0.07	.0014		0.06	0.41
ZrO_2	0.09	.0017		<0.05	<0.05
Nb_2O_5	<0.05	-		<0.05	2.18
BaO	0.19	.0028		0.17	0.28
La_2O_3	22.6	.3289		39.9 *	14.6
Ce_2O_3	29.9	.4321		25.5 *	23.2
Pr_2O_3	3.1	.0448		2.9 *	2.6
Nd_2O_3	10.4	.1466	1.0158	6.0 *	9.7
Sm_2O_3	1.10	.0149		1.06*	1.15
Eu_2O_3	0.22	.0031		<.2 *	<.2
Gd_2O_3	0.76	.0099		0.37*	0.52
Dy_2O_3	<.2	-		0.20*	0.51
Yb_2O_3	<.15	-		<.15*	<.15
ThO_2	3.21	.0289		<0.07	2.42
UO_2	0.08	.0007		0.09	0.11
TOTAL	101.26			101.75**	88.16
$\Sigma\left(\frac{REE_2O_3+}{Y_2O_3}\right)$	68.15			75.99*	52.69

\+ All Fe as FeO
* As wt% element
** Includes semi-quantitative F value of 25 wt% element
*** Number of cations based on 4 oxygens

normalized pattern shown in Fig. 5*c*. A semi-quantitative value of 25 % F was obtained using the Jeol 733 Superprobe.

Bastnäsite. The third rare earth mineral intergrown with monazite and fluocerite is bastnäsite. It occurs as dark, nearly opaque grains up to 250 μm in diameter. X-ray elemental distribution maps show a heretogeneous distribution of Fe and Ti, suggesting that bastnäsite is intergrown with Fe–Ti minerals. Although an X-ray powder diffraction photograph of the area analysed did not reveal the presence of minerals other than bastnäsite, the pattern obtained was very weak owing to the small amount of material sampled. The microprobe analysis given in Table 3 is an average of four spot analyses but, because of the heterogeneous nature of the grain, the analysis probably includes a component from intergrown Fe–Ti minerals. However, the *REE* concentrations in the Fe–Ti minerals are unlikely to make a significant contribution to the chondrite-normalized *REE* pattern (Fig. 5*c*), which is therefore considered to be that of bastnäsite. The *REE* composition compares most closely with that of the average of bastnäsites from granite pegmatites and granites (Fleischer, 1978).

Acknowledgements

We are grateful to Dr G. Love (Dept. of Materials Science, University of Bath) for the assistance on, and use of the Jeol 733 Superprobe, which is an SERC-funded instrument. Thanks are also due to Mr J. G. Francis and Dr J. E. Chisholm (British Museum, Natural History) for the X-ray powder diffractometry and assistance with their interpretation. Thanks also to colleagues in the Dept. of Mineralogy (BMNH) and an unknown reviewer for comments which have improved the manuscript. RGP also acknowledges support for the project from NSERC operating grant A9169.

References

Åmli, R., and Griffin, W. L. (1975) Microprobe analyses of *REE* minerals using empirical corrections. *Am. Mineral.* **60,** 559–606.

Borodin, L. S., Bykova, A. B., Kapitonova, T. A., and Pyatenko, Yu. A. (1960) New data on zirconolite and its niobium variety. *Dokl. Acad. Sci. USSR, Earth Sci. Sect.* **134,** 1022–4.

Calvo, C., and Faggiani, R. (1974) A re-investigation of the crystal structures of chevkinite and perrierite. *Am. Mineral.* **59,** 1277–85.

Fleischer, M. (1978) Relative proportions of the lanthanides in minerals of the bastnaesite group. *Can. Mineral.* **16,** 361–3.

——and Altschuler, Z. S. (1969) The relationship of the rare-earth composition minerals to geological environment. *Geochim. Cosmochim. Acta,* **33,** 725–32.

Fowler, M. B., and Williams, C. T. (1986) Zirconolite from the Glen Dessarry syenite; a comparison with other Scottish localities. *Mineral. Mag.* **50,** 326–8.

Frondel, J. W. (1975) *Lunar Mineralogy,* Wiley-Interscience, New York, 323 pp.

Gatehouse, B. M., Grey, I. E., Hill, R. J., and Rossell, H. J. (1981) Zirconolite, $CaZr_xTi_{3-x}O_7$; structure refinements for near end-member compositions with x = 0.85 and 1.30. *Acta Crystallogr.* **B37,** 306–12.

Gmelin Handbook of Inorganic Chemistry (A8, 1984) Y, *La, and the Lanthanoids: Minerals (Silicates). Deposits. Mineral Index.* (I. Kubach, ed.). Springer-Verlag, 248 pp.

Ito, J. (1967) A study of chevkinite and perrierite. *Am. Mineral.* **52,** 1094–104.

——and Arem, J. E. (1971) Chevkinite and perrierite: synthesis, crystal growth and polymorphism. Ibid. **56,** 307–19.

Kesson, S. E., and Ringwood, A. E. (1983) Safe disposal of spent nuclear fuel. *Rad. Waste Manag. and the Nucl. Fuel Cycle,* **4,** 159–74.

——Sinclair, W. J., and Ringwood, A. E. (1983) Solid solution limits in SYNROC zirconolite. *Nucl. Chem. Waste Manag.* **4,** 259–65.

Mazzi, F., and Munno, R. (1983) Calciobetafite (new mineral of the pyrochlore group) and related minerals from Campi Flegrei, Italy; crystal structures of polymignyte and zirkelite: comparison with pyrochlore and zirconolite. *Am. Mineral.* **68,** 262–76.

Mitchell, R. S. (1973) Metamict minerals: a review. Part II. Origin of the metamictization, methods of analysis, miscellaneous topics. *Mineral. Record,* **4,** 214–23.

Platt, R. G., and Woolley, A. R. (1986) The mafic mineralogy of the peralkaline syenites and granites of the Mulanje complex, Malawi. *Mineral. Mag.* **50,** 85–99.

Purtscheller, F., and Tessadri, R. (1985) Zirconolite and baddelyite from metacarbonates of the Oetztal-Stubai complex (northern Tyrol, Austria). Ibid. **49,** 523–9.

Raber, E., and Haggerty, S. E. (1979) Zircon oxide reactions in diamond-bearing kimberlites. In *Kimberlites, diatremes and diamonds: their geology, petrology and geochemistry* (F. R. Boyd and H. O. A. Meyer, eds). *Proc. Sec. Int. Kimberlite Conf.* **1,** 229–40.

Reed, S. J. B. (1986) Ion microprobe determination of rare earth elements in accessory minerals. *Mineral. Mag.* **50,** 3–15.

Ringwood, A. E. (1985) Disposal of high-level nuclear wastes: a geological perspective. Ibid. **49,** 159–76.

Roeder, P. L. (1985) Electron microprobe analysis of minerals for rare-earth elements: use of calculated peak-overlap corrections. *Can. Mineral.* **23,** 263–71.

Segalstad, T. V., and Larsen, A. O. (1978) Chevkinite and perrierite from the Oslo region, Norway. *Am. Mineral.* **63,** 499–505.

Shannon, R. D., and Prewitt, C. T. (1969) Effective ionic radii in oxides and fluorides. *Acta Crystallogr.* **B25,** 925–46.

Sinclair, W., and Ringwood, A. E. (1981) Alpha-recoil damage in natural zirconolite and perovskite. *Geochem. J.* **15,** 229–43.

Vlasov, K. A. (1966) In *Geochemistry and Mineralogy of Rare Elements and Genetic Types of their Deposits, Volume II, Mineralogy of the Rare elements* (K. A.

Vlasov, ed.). Israel Program for Scientific Translations, Jerusalem, 945 pp.

Wakita, H., Rey, P., and Schmitt, R. A. (1971) Abundances of the 14 rare earth elements and 12 other rare elements in Apollo 12 samples: five igneous and one breccia rocks and four soils. *Proc. Second Lunar Sci. Conf., Geochim. Cosmochim. Acta Suppl.* **2** (2), 1319–29.

Wark, D. A., Reid, A. F., Lovering, J. F., and El Goresy, A. (1973) Zirconolite (versus zirkelite) in lunar rocks (abstract). In *Lunar Science IV* (J. W. Chamberlain and C. Watkins, eds). Lun. Sci. Inst. Houston, 764–6.

White, T. J. (1984) The microstructure and microchemistry of synthetic zirconolite, zirkelite and related phases. *Am. Mineral.* **69,** 1156–72.

Williams, C. T. (1978) Uranium-enriched minerals in mesostasis areas of the Rhum layered pluton. *Contrib. Mineral. Petrol.* **66,** 29–39.

Woolley, A. R., and Garson, M. S. (1970) Petrochemical and tectonic relationship of the Malawi carbonatitic-alkaline province and the Lupata-Lebomba volcanics. In *African Magmatism and Tectonics* (T. N. Clifford and I. G. Gass, eds.). Oliver and Boyd, Edinburgh, 237–62.

——and Platt, R. G. (1986) The mineralogy of nepheline syenite complexes from the northern part of the Chilwa Province, Malawi. *Mineral. Mag.* **50,** 597–610.

[*Manuscript received 12 May 1986; revised 30 July 1986*]